Electron mobility and localization effects in high-density Ne gas

A. F. Borghesani and M. Santini
Dipartimento di Fisica "Galileo Galilei," Università di Padova, via F. Marzolo 8, I-35131 Padova, Italy
(Received 5 July 1990)

We report on the measurements of electron as well as ion mobility in neon gas at low temperature (close to the critical temperature) and up to very high density ($N \approx 180 \times 10^{20}$ cm^{-3}). We have found evidence of localized electron states at densities larger than $(90-100) \times 10^{20}$ cm^{-3}. The transition from the region of quasifree states to that of coexisting quasifree and localized states takes place in a density range in fairly good agreement with the predictions of a simple bubble model. The mobility data of the quasifree electron are in disagreement with the actual multiple-scattering theory. The detailed calculation of the mean mobility in the high-density region where localization takes place is still an unsolved problem.

I. INTRODUCTION

In this paper we report on the results of extra-electron mobility measurements in high-density neon gas, up to $N \approx 180 \times 10^{20}$ cm^{-3} (critical density $N_c = 144 \times 10^{20}$ cm^{-3}, critical temperature $T_c = 44.4$ K). To get such high densities we worked at temperatures close to the critical one ($T = 45.0$, 46.5, and 48.4 K).

Similar measurements in the range from 25 K to room temperature have been made in the past in our laboratory, but for densities not greater than 40×10^{20} cm^{-3}.[1] The results of these measurements raised a problem on the theoretical explanation of the electronic mobility within the multiple-scattering theories.[2,3] The density dependence of mobility could be explained only by introducing the assumption that the momentum-transfer cross section $\sigma_{MT}(\varepsilon)$ is to be evaluated at a shifted energy $\varepsilon' = \varepsilon + \varepsilon_0$, where ε_0 is a density-dependent "potential" to be determined. This effect, small when σ_{MT} is almost constant, is rather strong for neon, where σ_{MT} depends strongly on ε, particularly at low energies.[4] By using for ε_0 an iterated Wigner-Seitz potential, it is possible to get a good fit to all data between 25 K and room temperature without introducing any adjustable parameters. The situation lacks, however, a firm theoretical explanation. Moreover, the higher-density region was still to be explored.

In those early experiments we never found evidence of localized states, not even in the vapor. It is well known, however, that such states exist not only in a variety of liquids, but also in high-density He and H_2 gas.[5] The *e*-Ne scattering length is very low, but theoretical calculations show that localization should be possible in the liquid phase,[6] and the experiments showed that the negative carriers have indeed a very low mobility, comparable to that of an electron bubble.[7,8] But it is also possible that the slow carriers were O_2 impurity ions,[9] and so the problem remained essentially unsolved. In fact, the attachment to O_2 molecules, always present as "impurities," is very effective at high densities. To discriminate between slow electrons and O_2^- ions, we measured the mobilities of both species at the same time while following their behavior as a function of the neon-gas density, and found evidence of localized states for densities greater than $N^* \approx 95 \times 10^{20}$ cm^{-3}.

II. EXPERIMENT

A. General details

The experimental apparatus is essentially the same as that used in the previous experiment,[1] and its schematic is shown in Fig. 1. The only changes are the introduction of a second preamplifier to integrate the ionic wave forms, and an improved thermomechanical coupling of the cell to the cryogenerator head in order to minimize the mechanical noise while keeping a satisfactory thermal contact. An important improvement has also been intro-

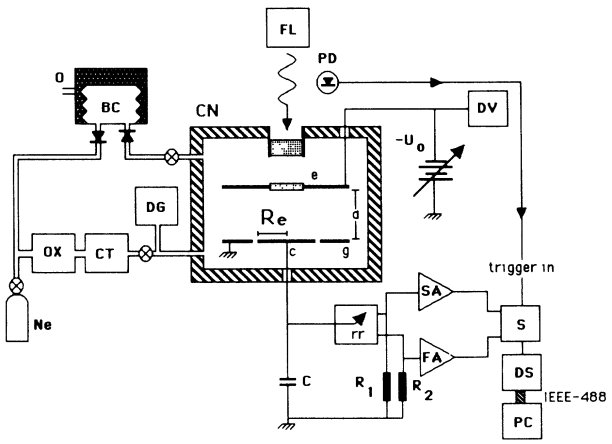

FIG. 1. Schematics of the experimental setup for electron- and ion-mobility measurements in neon gas: FL, xenon flash lamp; PD, photodiode; CN, copper cell; *e*, emitter; *c*, collector; *g*, guard ring; *d*, drift distance; $\mathcal{R}_e$, collector radius; DV, digital voltmeter; *C*, total integration capacitance; $R_1 = 10^{11}$ Ω, $R_2 = 10^9$ Ω, rr, reed relay; SA, slow amplifier; FA, fast amplifier; SA, selector switch; DS, digital scope; PC, personal computer; CT, liquid-nitrogen-cooled activated charcoal trap; OX, oxisorb trap, Ne, neon flask; *DG*, pressure gauge; IEEE-488, IEEE-488 interface bus.

duced in the analysis of the signal wave form.

A massive brass cell (≈ 1.5 kg weight) can withstand pressures up to 10 MPa. It can be cooled down to 25 K by a cryogenerator[10] and can be thermoregulated to within 0.01 K by means of standard techniques. The gold-plated emitter and collector electrodes are circular with a radius $\mathcal{R}_e = 3$ cm and are mounted inside the cell separated by a gap d, the drift distance. We usually used $d = 1$ cm, while at the highest densities we reduced d to ≈ 0.4 cm. The central area of the emitter is made by a small fused-silica disk coated with 100 Å Au, and it acts as the active area of the emitter. The electrons are extracted from the Au film by a xenon flash-lamp light pulse, which enters the cell through a thick fused-silica window.[1,11] The neon gas can be continuously circulated at high pressure in the closed circuit composed by the cell, the circulator, and the purifying traps. We used two such traps: an activated charcoal trap at 77 K and an Oxisorb one.[12] The bellow circulator is driven by pressurized oil.[13] More technical details on the whole experimental apparatus can be found in published papers.[1,11,13]

In the previous experiment the cell was directly fixed on the cold cryogenerator post to assure a good thermal contact. In such a way the reciprocating displacer of the cryogenerator head induces vibrations in the electrodes assembly, causing an output electrical noise proportional to the potential difference applied to the electrodes. In the present experiment it was necessary to use also high voltages (up to 2500 V), and the noise voltage induced by the displacer was so high as to prevent any measurements. To remove this trouble, the cell was coupled in a softer way to the cold post, through a kind of spring made by four copper strips, mounted as shown in Fig. 2. Because the cell is massive, we get a very low resonant frequency even with rather thick strips, allowing for a good mechanical filtering of the vibrations with still a satisfactory thermal contact.

B. Electronics

The collector can be connected via a reed switch to the *slow* amplifier SA, or to the *fast* amplifier FA (Fig. 1). It can be shown that, for a good reproduction of the wave forms, one gets the best signal-to-noise ratio and also the highest possible signal if one integrates the current $i(t)$ induced by the charges moving in the drift space.[14] The integration is performed by the group R_1C or R_2C at the input of the amplifiers. These are placed close to the cell in order to minimize the total capacitance C ($C \approx 50$ pF). The *fast* amplifier has an input resistance $R_2 = 10^9\ \Omega$ ($R_2C \approx 50 \times 10^{-3}$ s), and is used to integrate and amplify the signals induced by the fast electrons. To integrate the ionic signals, which may last some tenths of a second or more, we need a much larger time constant. Using the operational amplifier OPA 128,[15] which shows a very low input bias current (100×10^{-15} A, typically) it is possible to use a larger input resistance $R_1 = 10^{11}\Omega$ ($R_1C \approx 5$ s). We can therefore record both the electronic and the ionic parts of the signal wave form. The output signals are recorded by a digital storage oscilloscope (Hitachi VC-6041) and are fetched and stored by a personal computer (Macintosh II) to allow off-line data processing.

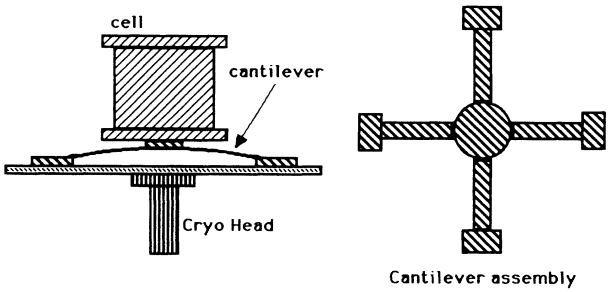

FIG. 2. Mechanical coupling of the cell to the cryogenerator head by means of four copper cantilevers.

III. SIGNAL WAVE FORMS

The signal wave forms may look rather different from each other, depending on the physical situation. A detailed wave-form analysis and the description of the numerical methods exploited to extract the information of interest can be found elsewhere.[14] We summarize here only the main results.

A. Fast wave forms

The general wave form has a fast initial part, followed by a slower one. We begin first with the fast part. Let U_0 be the potential of the emitter with respect to the collector and $E_0 = U_0/d$ the electric field applied to the drift region. The time of flight for electrons and O_2^- ions will be respectively $\tau_e = d/\mu_e E_0$ and $\tau_i = d/\mu_i E_0$, where μ_e and μ_i are the respective mobilities for that field. If $n_e(t)$ is the number of electrons at time t, then the induced electric current is $i_e(t) = -en_e(t)/\tau_e$. If a short bunch of n_0 electrons is injected into the drift space, the current will be

$$i_e(t) = -\frac{en_0}{\tau_e} e^{-t/\tau}, \tag{1}$$

where e is the elementary charge, $\tau = 1/\nu_A$ is the mean lifetime of quasifree electrons, and ν_A is the attachment frequency. The relation (1) holds under the following conditions:

(i) For electrode radius $\mathcal{R}_e \gg d$. A detailed analysis shows that $\mathcal{R}_e \geq 2.5d$ can be satisfactory.[16]

(ii) Space charge effects are absent. This means $E = E_0$, constant along the whole drift space.

(iii) $\tau_i \gg \tau_e$. This last condition is usually well fulfilled, except at the highest neon densities, where μ_e becomes very low. In this case we cannot neglect the contribution of the ionic current to the first "fast" part of the wave form, and the relation (1) should be modified (see Appendix A).

The integrated wave form (for $RC \gg \tau_e$) is given by

$$v_e(t) = -\frac{v_T}{A}(1 - e^{-\nu_A t}), \tag{2}$$

where $v_T = en_0/C$ is the maximum available voltage, i.e., $v_T = v_e(\tau_e)$ for $A = 0$. The attaching efficiency $A = \tau_e/\tau = \nu_A \tau_e$ gives a measure of the efficiency of the electron attachment to O_2 molecules. For $t = \tau_e$, $v_e(\tau_e) = v_S = -(v_T/A)[1 - \exp(-A)]$. When $A \gg 1$ (strong attachment) the wave form is practically an exponential decay towards v_S. In this case one can measure only the attachment frequency ν_A. To measure τ_e one needs a better purification, or a stronger field E (in order to reduce τ_e). When $A \ll 1$, the wave form (2) becomes a straight line and τ_e can be measured very well. At high densities one has usually an intermediate situation, and it is possible to get both τ_e and ν_A from a proper analysis of the wave form.[14] To examples of fast wave forms are shown in Fig. 3.

B. Slow wave forms

Once the fast electrons have been collected, very slow ions are still left in the drift space. This ionic distribution can be easily calculated. It moves slowly towards the collector. If $n_i(t)$ is the total number of ions still present at the time t, then $i_i(t) = -en_i(t)/\tau_i$. Assuming $\tau_e = 0$, because $\tau_i \gg \tau_e$, the ionic current can be found to be[14]

$$i_i(t) = -(en_0/\tau_i)(1 - e^{A(t/\tau_i - 1)}) . \quad (3)$$

The relation (3) holds under the same conditions imposed to relation (2). The condition $\tau_i \gg \tau_e$ can be unvalid at high densities, and the relation (3) must be modified (see Appendix A).

If $RC \gg \tau_i$, the integrated wave form for $\tau_e \le t \le \tau_i$ is found to be

$$v_i(t) = -v_T \left[\frac{1}{A} + \frac{t}{\tau_i} - \frac{e^{-A}}{A} e^{At/\tau_i} \right] . \quad (4)$$

Because $\tau_e \ll \tau_i$, $v_i(\tau_e) = -(v_T/A)(1 - e^{-A})$, which is exactly equal to $v_e(\tau_e) = v_S$. For $t = \tau_i$, $v_i(\tau_i) = -v_T$, and so $v_i(\tau_e)/v_i(\tau_i) = (1 - e^{-A})/A$. From this relation one easily gets the attachment efficiency $A = \nu_A \tau_e$, and if τ_e is measured from the fast wave form, ν_A can be easily determined.

When one needs to work at low electric fields, τ_i can increase up to 1 s or more, and, therefore, the condition $RC \gg \tau_i$ is no longer satisfied. In such a situation, for $\tau_e \le t \le \tau_i$ we have

$$v(t) = -v_T(I - P^{-t/RC} - Qe^{At/\tau_i}) , \quad (5)$$

where $I = RC/\tau_i$, $P = [e^{-A} + (AI)^2 - 1]/[A(1 + AI)]$, and $Q = [Ie^{-A}/(1 + AI)]$. For $t \ge \tau_i$, $v(t) = v(\tau_i)\exp[-(t - \tau_i)/RC]$. If $AI > 1$, the wave form has a minimum for $t_M < \tau_i$. Two examples of slow wave forms are shown in Fig. 4. The methods for calculating τ_i and A from the slow wave forms are described in de-

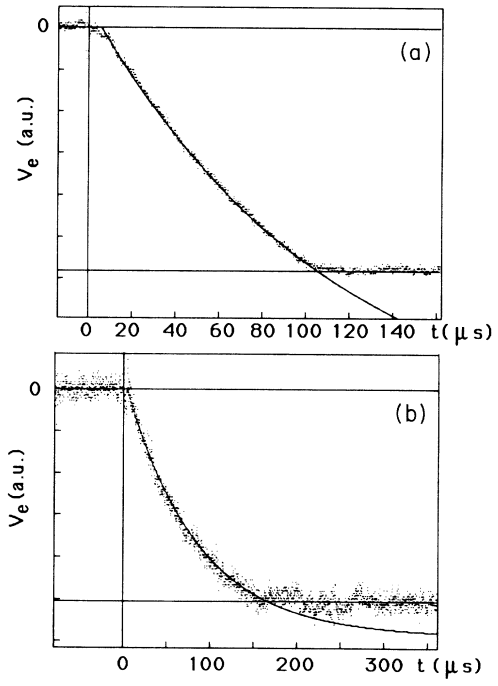

FIG. 3. Typical electronic (fast) wave forms. The experimental conditions under which the signals were recorded are the following: (a) $T = 150$ K, $N = 27.3 \times 10^{20}$ cm^{-3}, $E_0 = 15$ V/cm, $E_0/N = 54.9 \times 10^{-22}$ V cm^2, $\nu_A = 14.7$ kHz, $\tau_e = 97.0$ μs, $A = 1.43$. (b) $T = 150$ K, $N = 22.5 \times 10^{20}$ cm^{-3}, $E_0 = 3.0$ V/cm, $E_0/N = 13.3 \times 10^{-22}$ V cm^2, $\nu_A = 11.3$ kHz, $\tau_e = 172$ μs, $A = 1.94$.

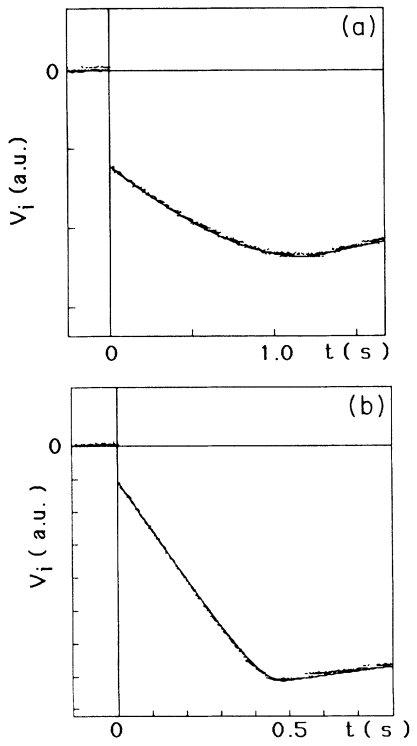

FIG. 4. Typical ionic (slow) wave forms. The experimental conditions under which the signals were recorded are the following: (a) $T = 89.8$ K, $N = 41.4 \times 10^{20}$ cm^{-3}, $E_0 = 40.6$ V/cm, $E_0/N = 98.1 \times 10^{-22}$ V cm^2, $A = 1.98$, $AI = 7.8$, $\tau_i = 1.260$ s. (b) $T = 89.8$ K, $N = 64.1 \times 10^{20}$ cm^{-3}, $E_0 = 140.0$ V/cm, $E_0/N = 218.4 \times 10^{-22}$ V cm^2, $A = 6.93$, $AI = 70.7$, $\tau_i = 0.488$ s.

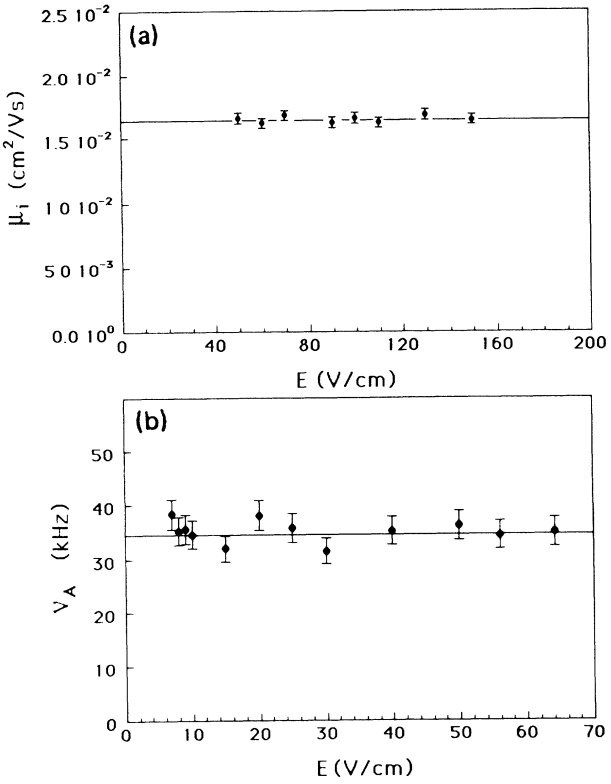

FIG. 5. (a) O_2^- mobility μ_i vs electric-field strength in Ne gas at $T=48.4$ K and $N=52.2\times10^{20}$ cm^{-3}. (b) Attachment frequency ν_A vs electric-field strength at $T=170.3$ K and Ne-gas density $N=27.7\times10^{20}$ cm^{-3}. Error bars represent ±1 standard deviation.

tail in our paper.[14] In Fig. 5 we report two examples of results for ν_A and μ_i obtained by these methods.

IV. EXPERIMENTAL RESULTS

Once the cell has been cooled at the selected temperature, it is filled with neon gas at the working pressure. The gas is forced to circulate through the Oxisorb trap and through the activated charcoal cold trap to remove oxygen and nitrogen impurities. The purity degree can be estimated from the signal wave form. At high densities a very low impurity concentration must be reached, and the circulation has to last a few hours. As a result the typical attachment frequency is in the range 0.5–10 kHz.

We worked at three temperatures, 45.0, 46.5, and 48.4 K. At each temperature and at a fixed density N we measured the mobility as a function of the electric field E down to the lowest attainable values of E, in order to determine the "zero-field mobility" μ_0. The results for μ_0 versus N are shown in Fig. 6. The numerical density N has been calculated by means of the equation of state given by McCarty and Stewart.[17] At the same time we have plotted also the values obtained for the ionic mobility μ_i. These slow carriers are oxygen ions O_2^-. In fact, when the gas is circulated for an extended period of time through the oxygen adsorber Oxisorb, the slow component of the wave form becomes smaller, while the fast

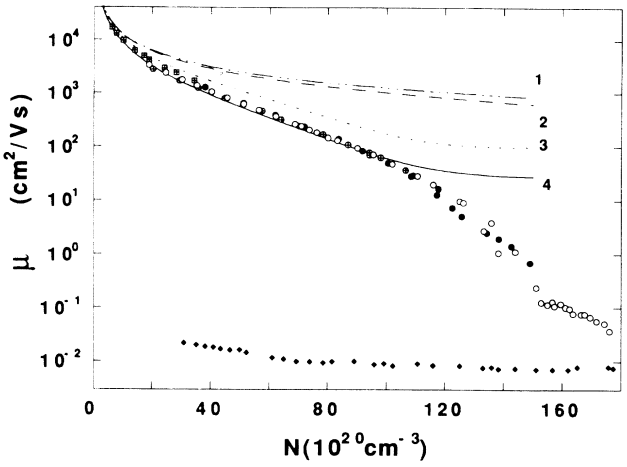

FIG. 6. Experimental results for the electron and ion mobilities as a function of the neon-gas density. Crossed squares, $T=47.9$ K; crossed circles, $T=45.0$ K; solid circles, $T=48.4$ K; open circles, $T=46.5$ K; solid diamonds, O_2^--ion mobilities at 45.0–48.4 K. Curve 1, classical mobility [Eq. (6)]; curve 2, O'Malley formula, which takes into account multiple-scattering effects (see text); curve 3; Lorentz-Lekner formula [Eq. (7)]; curve 4; mobility calculated according to formula (7) with the σ_{MT} evaluated at the shifted energy $\varepsilon'=\varepsilon+\varepsilon_{WS}$, with ε_{WS} given by relation (18).

electronic one increases.

We see from the figure that at a density N^* between 90×10^{20} and 100×10^{20} cm^{-3} there begins a gradual increase of the slope of the plot of $\ln\mu_e$ versus N, with a change of curvature. We believe that for $N<N^*$ only extended states exist (quasifree electrons), while for $N>N^*$ we have the coexistence of both extended and localized states (bubbles), with a gradual disappearing of quasifree electrons as the density increases. This explanation is confirmed by the dependence of μ_e on E at the various densities shown in Fig. 7. When $N<N^*$, μ_e decreases with E and gradually recovers the classical $E^{1/2}$ dependence at high E, as in our previous work.[1] When

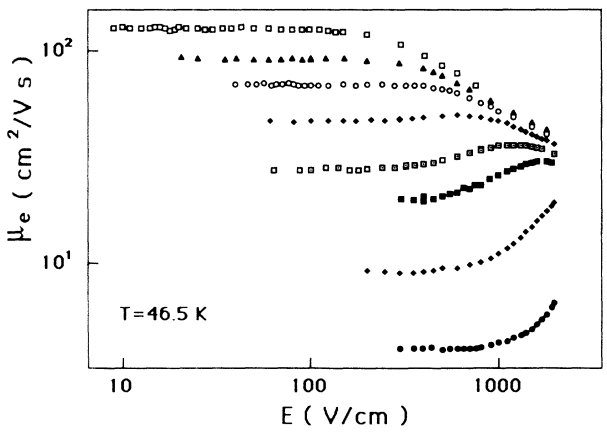

FIG. 7. Electric field dependence of the electronic mobility at $T=46.5$ K for several densities. From top to bottom: $N=83.4$, 90.2, 95.6, 102.1, 110.8, 116.1, 126.3, and 135.9 ($\times10^{20}$ cm^{-3}).

$N > N^*$, μ_e first increases with E, it goes through a maximum and then meets the classical high-E dependence. We can see in Fig. 8 that the behavior changes at a density N^* between 90×10^{20} and 100×10^{20} cm^{-3}. The qualitative explanation is that for $N > N^*$ and at low electric fields there is coexistence of quasifree and localized electron states, in the sense that the electrons are quasifree for a mean time τ_F, and they are localized for a mean time τ_B. The average mobility should be given by $\bar{\mu}=(\tau_F/\tau_s)\mu_F+(\tau_B/\tau_s)\mu_B$, where μ_F and μ_B are the mobilities of the quasifree and localized states, respectively, and $\tau_s=\tau_F+\tau_B$. The electric field can inhibit the initial trapping of the electrons in a density fluctuation, or enhance their escape from stable localized states, or both. In any way, the ratio τ_F/τ_B can be increased with increasing E. At densities close to N^* the binding energy of the localized state is low and a detectable effect on τ_F/τ_B can be achieved with rather small fields. At higher densities the localized states are more stable and therefore we see an effect only at higher fields. In order to summarize the experimental results we may pick out, from the plots like those in Fig. 8, the value E^* of the electric field at which the mobility begins to increase over its low-field value. The E^* values are plotted in Fig. 9 as a function of N. Because this method is a very rough one, E^* can be identified only with rather large uncertainty. Nonetheless, we clearly see that E^* increases rapidly with N. A qualitative fit of this data shows that E^* goes to zero for $N^*\approx95\times10^{20}$ cm^{-3}. In Sec. V B we will see that a simple bubble model indicates that localized states are possible only for densities greater than N^* in agreement with the mobility results.

V. DISCUSSION

A. Quasifree electrons

At very low densities the zero-field electronic mobility μ_0 is given by the well-known classical relation

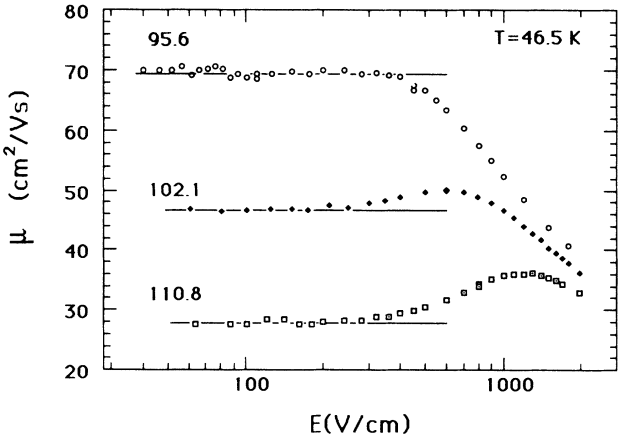

FIG. 8. Expanded view of the electric-field dependence of the electron mobilities at $T=46.5$ K for the three density values $N=95.6$, 102.1, and 110.8×10^{20} cm^{-3}. From this figure we can see that for $N\geq95\times10^{20}$ cm^{-3} there is a value of the field strength E^* for each density at which the mobility increases over its low-field value before reaching the $E^{1/2}$ behavior.

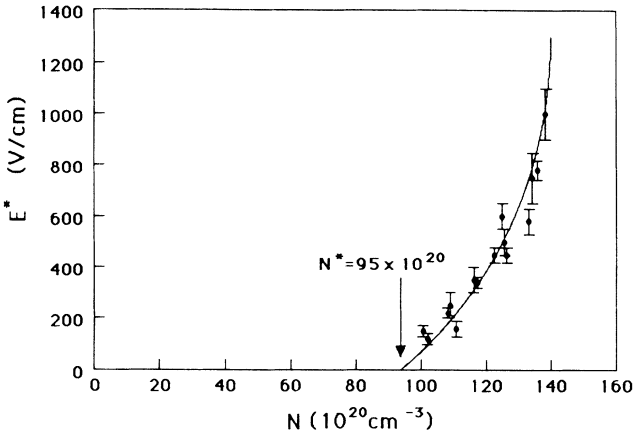

FIG. 9. Plot of the E^* values as a function of the neon-gas density.

$$\mu_{\rm cl}=\frac{B(T)}{N(k_BT)^2}\int_0^\infty\frac{\varepsilon\exp(-\varepsilon/k_BT)}{\sigma_{\rm MT}(\varepsilon)}d\epsilon\ , \tag{6}$$

with $B(T)=\frac{4}{3}e(2\pi mk_BT)^{-1/2}$, where e is the elementary charge, m is the electron mass, k_B is the Boltzmann constant, and $\sigma_{\rm MT}(\varepsilon)$ is the energy-dependent electron-atom momentum-transfer cross section. We use as in our previous work the cross section given by O'Malley and Crompton.[4] Values calculated from (6) are plotted in Fig. 6 for $T=46.5$ K (curve 1). It is well known that the classical relation is inadequate at high densities. In our case, as an example, for $N\approx90\times10^{20}$ cm^{-3} the classical relation gives a value about 160 times larger than the measured one. At this density, however, the isothermal compressibility χ_T calculated from the state equation[17] turns out to be 5.8 times larger than that of the ideal gas, and therefore the correlations between scatterers cannot be ignored. To take them into account we may use the result of Lekner,[18] and we can divide the classical relation (6) by $S(0)=(Nk_BT)\chi_T$, the long-wavelength part of the structure factor $S(k)$, in order to get the so-called Lorentz-Lekner formula

$$\mu_{\rm LL}=\frac{\mu_{\rm cl}}{(Nk_BT)\chi_T(N,T)}\ . \tag{7}$$

where $\chi_T(N,T)$ is the density and temperature-dependent isothermal compressibility. The values of $\mu_{\rm LL}$ for $T=46.5$ K are shown in Fig. 6, curved 3, and are still higher than the experimental data.

It is also well known that at high densities, multiple-scattering effects must be taken into account. Many theoretical attempts have been made in order to explain the experimental results obtained in several gases.[19] For densities not too high, as an example, the result of O'Malley[3] for gases with positive scattering length is essentially a final relation like the classical relation (6), where the exponential inside the integral is modified as $\exp\{-[\varepsilon+\Gamma(\varepsilon)]/(k_BT)\}$, with

$$\Gamma(\varepsilon)=[2\hbar/(2m)^{1/2}]N\sigma_T(\varepsilon)\sqrt{\varepsilon}\ ,$$

where $\sigma_T(\varepsilon)$ is the total electron-atom cross section. By using an entirely different approach, Braglia and Dallaca-

sa obtained essentially the same result for densities not too high.[2] Values calculated by this way are given by curve 2 in Fig. 6. We see that these theories, at least for the case of neon, introduce only a small correction to the classical theory, because the electron-neon scattering cross section is low. This fact was clearly shown in our previous paper at lower densities and is confirmed also by our new results at high densities. If we divide the results by $S(0)$ as explained before, we get values slightly smaller than those of curve 3, but still higher than the experimental values. For higher densities the result of Braglia and Dallacasa is similar to the Legler relation,[20] but corrected for the localized states [formula (5.6), Ref. 2]. Values calculated in this way are shown in Fig. 10, by neglecting the scatterers correlations (curve 1) as well as by taking them into account through the structure factor $S(0)$ (curve 2). We believe that this disagreement is peculiar to neon because the cross section is so small and strongly energy dependent, particularly at low energies. The multiple-scattering result was obtained for essentially constant cross sections, and therefore they neglect a possible effect arising from both the quantum shift of the electron energy and the energy dependence of the cross section. From an accurate analysis of the data we arrived, in the previous work, at the conclusion that it seems reasonable to assume that the scattering cross section $\sigma_{MT}(\varepsilon)$ which appears in the relation (6) should be calculated at some shifted energy $\varepsilon'=\varepsilon+\varepsilon_0$, where ε_0 depends only on the scatterer density N. In that paper[1] we calculated ε_0 with the Wigner-Seitz model, using for the effective radius a a kind of "self-consistent" radius given by $a=[\sigma_T(\varepsilon_0)/4\pi]^{1/2}$, using the total-scattering cross section of O'Malley and Crompton.[4] This energy shift ε_{WS} (iterated Wigner-Seitz energy shift) is shown in Fig. 11 as a function of N. It can be well interpolated by the

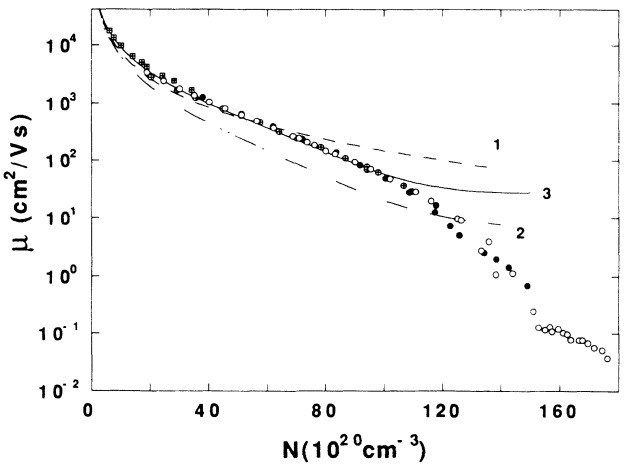

FIG. 10. Experimental results for the electron mobility along with several theoretical formulas. Curve 1; Braglia and Dallacasa (Ref. 2) results obtained by neglecting correlations among the scatterers. Curve 2; same as curve 1 but divided by the static structure factor $S(0)$, in order to account for such correlations. Curve 3: Lorentz-Lekner results [relation (7)] but taking into account the energy shift calculated according to the corrected Fermi model [Eq. (12)].

following relation:

$$\varepsilon_{WS}=0.540N+4.88\times10^{-2}N^{3/2}+2.46\times10^{-3}N^2\ , \tag{8}$$

where ε_{WS} is measured in meV and N in units of 10^{20} cm^{-3}. The mobility calculated by this way reproduced well the data up to $N=40\times10^{20}$ cm^{-3} in a wide temperature range.

If we use the same procedure for the present experiment, while using the Lorentz-Lekner relation (7), we get curve 4 in Fig. 6, which fits rather well our data up to N^*.

It has to be said, however, that such a calculation for ε_0 is quite arbitrary and not theoretically justified. We want to show here that the choice of a particular ε_0 is not unique and that a different model can be constructed which moreover gives even a better fit to the experimental data.

Indeed, in the multiple-scattering theory the energy shift is given by the equation[21]

$$\varepsilon_0=-N\frac{2\pi\hbar^2}{m}f_k^0(\varepsilon_0)\ , \tag{9}$$

where f_k^0 is the real part of the forward-scattering amplitude[22]

$$f_k^0(\varepsilon)=\sum_{l=0}^{\infty}\frac{(2l+1)\sin[2\eta_l(\varepsilon)]}{2k(\varepsilon)}\ , \tag{10}$$

where $k(\varepsilon)$ is the electron wave vector. For low N (and small ε_0) the relation (9) gives the well-known Fermi shift $\varepsilon_F=(2\pi\hbar^2/m)Na$,[23] which for positive scattering length can be written as

$$\varepsilon_F=\frac{\pi^{1/2}\hbar^2}{m}[\sigma_T(0)]^{1/2}N\ . \tag{11}$$

The calculation of ε_0 through (9) and (10), using the phases η_0 through η_5 given by O'Malley and Crompton,[4] shows that ε_0 given by (9) is very close to the Fermi shift ε_F. For $N=100\times10^{20}$ cm^{-3}, for instance, it is only 12% larger than ε_F. If we approximate ε_0 with ε_F, and try to take the correlations into account by using an effective cross section $\sigma^*=S(0)\sigma_T(0)$ in Eq. (11), we get a kind of "corrected Fermi shift" $\varepsilon_{FC}=\varepsilon_F[S(0)]^{1/2}$,

$$\varepsilon_{FC}=0.540N[S(0)]^{1/2}\ , \tag{12}$$

with ε_{FC} in meV and N in units of 10^{20} cm^{-3} (see Fig. 11). If we use now this shift for $\sigma_{MT}(\varepsilon)$ in the Lorentz-Lekner relation (7), we get curve 3 in Fig. 10. The goodness of this fit is comparable (or even better) to that given by curve 4 in Fig. 6, obtained with the use of the iterated Wigner-Seitz shift ε_{WS}.

To conclude, our new data confirm the qualitative idea that the momentum-transfer cross section $\sigma_{MT}(\varepsilon)$ has to be calculated at a shifted energy $\varepsilon'=\varepsilon+\varepsilon_0$. How to calculate this shift in a theoretically sound way remains an open question.

B. Localized states

In this section we show that the simple bubble model[24] indicates that stable localized states are possible, at the

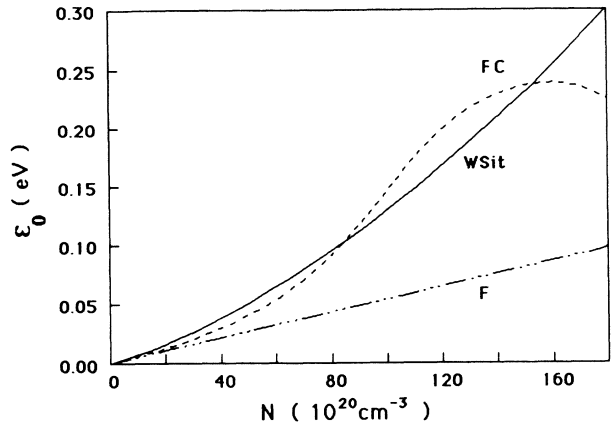

FIG. 11. Energy shift ε_0 calculated according to Eq. (11) (curve F), to Eq. (12) (curve FC at $T=46.5$ K), or to the iterated Wigner-Seitz model.

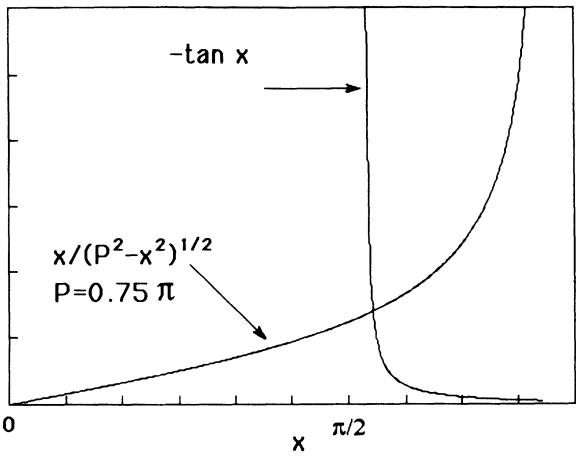

FIG. 12. Sketch of the rhs and lhs of Eq. (15) for the electron in the spherical well. It can be seen that there are solutions only if the potential well strength $H=P$ satisfies the condition $H \geq \pi/2$.

temperatures of our experiment, for densities greater than $N^* \approx 95\times 10^{20}$ cm^{-3}, in agreement with the experimental results.

Suppose that electrons are subjected to a spherical potential with $V=V_i$ for $r<\mathcal{R}$ and $V=V_0$ for $r>\mathcal{R}$ ($V_i<V_0$). If the lowest bounded state exists (with quantum numbers $n=1$, $l=0$) with energy $\mathcal{E}_1$ and wave function $u(r)$, it is well known that the function $f(r)=ru(r)$ must fulfill the radial equation

$$f''+k_i^2 f=0 \quad \text{for } r\leq\mathcal{R} ,$$

$$f''-k_0^2 f=0 \quad \text{for } r>\mathcal{R} ,$$

where $f''=\partial^2 f/\partial r^2$, and

$$k_i^2=\frac{2m}{\hbar^2}(\mathcal{E}_1-V_i) , \tag{13}$$

$$k_0^2=\frac{2m}{\hbar^2}(V_0-\mathcal{E}_1) . \tag{14}$$

From the boundary conditions imposed on the radial wave functions $u_i(r)$ and $u_0(r)$, at $r=\mathcal{R}$, one gets the equation

$$-\tan X=\frac{X}{(H^2-X^2)^{1/2}} , \tag{15}$$

where

$$X=k_i\mathcal{R} \tag{16}$$

and

$$H^2=\frac{2m}{\hbar^2}(V_0-V_i)\mathcal{R}^2 . \tag{17}$$

If $X_1=(k_i)_1\mathcal{R}$ is the solution of (15), then the energy $\mathcal{E}_1$ of the s state will be, from (13),

$$\mathcal{E}_1=\frac{\hbar^2}{2m\mathcal{R}^2}X_1^2+V_i . \tag{18}$$

The right-hand side (rhs) of (15) is always positive and approaches ∞ for $X\rightarrow H$, and therefore there are no solutions if $H<\pi/2$ (see Fig. 12). In order to have a bound state, it should be $H>\pi/2$, or from (17),

$$\frac{2m\mathcal{R}^2}{\hbar^2}(V_0-V_i)>\frac{\pi^2}{4} . \tag{19}$$

1. *The empty bubble*

In this model the electron is trapped in an empty spherical cavity of radius $\mathcal{R}$. Let T be the absolute temperature, N the number density of the host gas, and $P=P(N,T)$ the gas pressure given by the state equation. The potential for $r>\mathcal{R}$ is the density-dependent self-energy $V_0(N)$. For $r<\mathcal{R}$ we must account for the polarization energy $V_P(r)$, which depends slightly on r. As a first approximation we may take $V_P=$const, and calculate it for $r=0$.[6] In this case $V_P=-(\alpha e^2/2)\int_{\mathcal{R}}^{\infty}(4\pi r^2 N/r^4)dr=-\mathcal{E}_P N/\mathcal{R}$, with $\mathcal{E}_P=2\pi\alpha e^2$, where $\alpha=0.392\times 10^{-24}$ cm^{-3} is the atomic polarizability of neon. If the density N is fixed we have therefore

$$V_i=-\frac{\mathcal{E}_P N}{R}, \quad V_0=V_0(N) . \tag{20}$$

The radius $\mathcal{R}_0$, below which there are no bound states, is given by Eq. (19), which together with (20) becomes

$$\frac{2m}{\hbar^2}V_0\mathcal{R}^2+\frac{2m}{\hbar^2}\mathcal{E}_P N\mathcal{R}-\frac{\pi^2}{4}=0 ,$$

with the solution

$$\mathcal{R}_0=\frac{1}{2V_0}\left[-N\mathcal{E}_P+\left[N^2\mathcal{E}_P^2+\frac{2m}{\hbar^2}V_0\pi^2\right]^{1/2}\right] . \tag{21}$$

For each $\mathcal{R}>\mathcal{R}_0$, and with H^2 given by (17), we find out the solution $X_1=X_1(\mathcal{R})$ of Eq. (15). The total energy $\mathcal{E}_T$ is given by (18) plus the volume energy $\mathcal{E}_V$ given by the work done (at constant temperature) against the pressure P to create the spherical cavity

$$\mathcal{E}_T=\frac{\hbar^2 X_1^2(\mathcal{R})}{2m\mathcal{R}^2}-\frac{\mathcal{E}_P N}{\mathcal{R}}+\mathcal{E}_V\ , \tag{22}$$

where for the empty bubble $\mathcal{E}_V+(4\pi/3)P\mathcal{R}^3$. If $\mathcal{E}_T(\mathcal{R})$ shows a minimum $\mathcal{E}_M$ for $\mathcal{R}=\mathcal{R}_M$, the localized state be stable, otherwise both $\mathcal{E}_T(R)$ and $\mathcal{R}$ decrease until, for $\mathcal{R}=\mathcal{R}_0$, the electron leaves the bubble.

However, the bubble can be unstable even if $\mathcal{E}_T(\mathcal{R})$ shows a minimum. In fact, if $\mathcal{E}_M > V_0$ the quasifree state is certainly favored. On the contrary, only if $V_0-\mathcal{E}_M \gg k_B T$ is the bubble state certainly stable. As a rough approximation, the number of localized electrons n_B and of quasifree electrons n_F are given by the ratio $n_B/n_F=\exp[-(\mathcal{E}_M-V_0)/k_B T]$. A detailed calculation shows that empty bubbles are very unlikely in neon. As an example, if we use for $V_0(N)$ the Wigner-Seitz potential (8), at $T=46.5$ K the empty bubble is stable only for densities $N > 137\times10^{20}$ cm^{-3}, and $\mathcal{E}_M=V_0$ $(n_B/n_F=1)$ only for $N > 175\times10^{20}$ cm^{-3}. This is due to the fact that the gas pressure is high in our case ($P\approx3.41$ MPa for $T=46.5$ K, $N\approx137\times10^{20}$ cm^{-3}), and the volume energy $\mathcal{E}_V$ is so large that it prevents the formation of stable bubbles.

2. *Partially empty bubble*

The density profile of the empty bubble is certainly unrealistic for a gas, and self-consistent methods can be used to calculate a softer profile which minimizes the total bubble energy.[25] Here we want to show with a very simple model that stable bubbles are possible even at high pressures if they are only partially empty.

As shown in Appendix B, the volume energy can be much smaller than PV in this situation. Let us therefore consider a model in which inside a spherical cavity of radius $\mathcal{R}$ there is a density $N_1=NF$, where F is the filling fraction of the cavity. The electron self-energy will be $V_0=V_0(N)$ for $r>\mathcal{R}$ and $V_1=V_0(N_1)$ for $r<\mathcal{R}$.

For the potential for $r<\mathcal{R}$ we take

$$V_i=V_1+V_P=V_0(N_1)-\frac{\mathcal{E}_P N}{\mathcal{R}}(1-F)\ , \tag{23}$$

where the polarization energy has been roughly corrected in such a way that $V_P\to0$ for $F\to1$ and $V_P=\mathcal{E}_P N/\mathcal{R}$ for $F=0$. At N, F, and $\mathcal{R}$ fixed, we have V_0 and V_i, and so $H^2=(2m/\hbar^2)[V_0-(V_1+V_P)]$. The condition $H^2\geq\pi^2/4$ allows us to calculate the minimum radius $\mathcal{R}_0$ as

$$\mathcal{R}_0=\frac{-N(1-F)\mathcal{E}_P+[N^2(1-F)^2\mathcal{E}_P^2+(2m/\hbar^2)(V_0-V_1)\pi^2]^{1/2}}{2(V_0-V_1)}\ . \tag{24}$$

For each $\mathcal{R}>\mathcal{R}_0$ we can calculate H^2, and we can find out numerically the solution $X_1=X_1(R)$ of Eq. (15). The total energy is still given by (22), where now the volume energy $\mathcal{E}_V$ is given by relation (B1) of Appendix B. It can be easily calculated if we know the equation of state $P=P(N,T)$ at the chosen temperature T. At each temperature T, however, the data calculated from the state equation can be well fitted to the cubic equation $P=AN+BN^2+CN^3$, at least in the density range of our interest. In this case $\mathcal{E}_V$ can be calculated directly from (B1) and it turns out to be

$$\mathcal{E}_V=\frac{4\pi}{3}P\left[(1-F)-\frac{FN}{P}[BN(1-F)+0.5CN^2(1-F^2)-A\ \ln F]\right]\ . \tag{25}$$

We now change $\mathcal{R}$ to find, if it exists, the minimum $\mathcal{E}_M$ of the total energy $\mathcal{E}_T(\mathcal{R})$. The dependence of $\Delta=(\mathcal{E}_M-V_0)/k_B T$ as a function of the filling factor F is shown in Figs. 13 for several densities at $T=46.5$ K. The calculations were done by using the Wigner-Seitz potential (8) as $V_0(N)$, and the equation of state of McCarty and Stewart.[17] The results of the model show that at low densities the bubble tends to get more and more filled to minimize its total energy, until no minimum exists for $\mathcal{E}_T$ as a function of $\mathcal{R}$. Electron bubbles at these densities, even if created by thermal fluctuations, cannot be stable. As the density is increased, the total energy $\mathcal{E}_M$ shows a minimum $\mathcal{E}_B$ for defined values $\mathcal{R}_B$ and F_B of bubble radius and filling factor. This minimum becomes more and more pronounced as the density is increased. In this situation the bubble can be stable against fluctuations of the

TABLE I. V_1, V_P, $\mathcal{E}_1$, $\mathcal{E}_V$, and $\mathcal{E}_M$ in meV, $\mathcal{R}_M$ in Å. The symbols are defined in the text.

F	V_1	V_P	$\mathcal{E}_1$	$\mathcal{E}_V$	$\mathcal{E}_M$	Δ	$\mathcal{R}_M$
0.1	8.9	−38.0	125.6	43.8	169.3	1.25	10.1
0.2	20.1	−28.9	115.5	41.1	156.5	−1.94	11.8
0.3	33.2	−22.3	112.7	36.0	148.6	−3.91	13.4
0.4	47.9	−16.8	113.5	30.9	144.5	−4.96	15.2
0.5	64.0	−12.4	117.9	25.5	143.4	−5.23	17.2
0.6	81.5	−8.7	124.4	20.5	144.9	−4.84	19.7
0.7	100.3	−5.56	133.1	15.6	148.7	−3.91	23.0
0.8	120.4	−3.04	143.2	10.9	154.1	−2.55	28.0
0.9	141.8	−1.14	154.6	5.76	160.4	−0.98	37.4

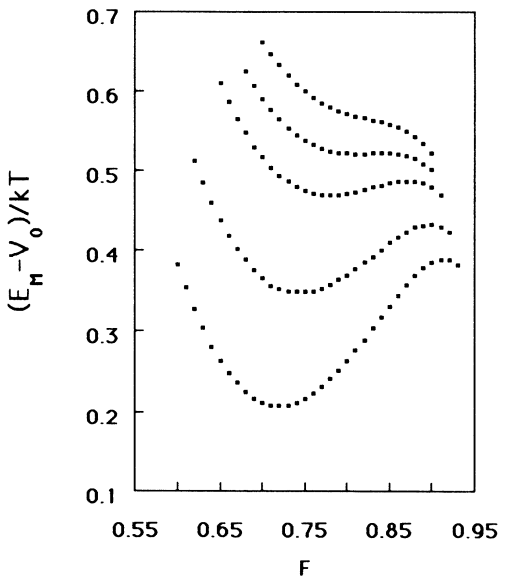

FIG. 13. The dependence of Δ as a function of the filling factor for neon gas at $T=46.5$ K and at several densities. From top to bottom: $N=95.0$, 95.5, 96.0, 97.0, and 98.0 ($\times 10^{20}$ cm^{-3}).

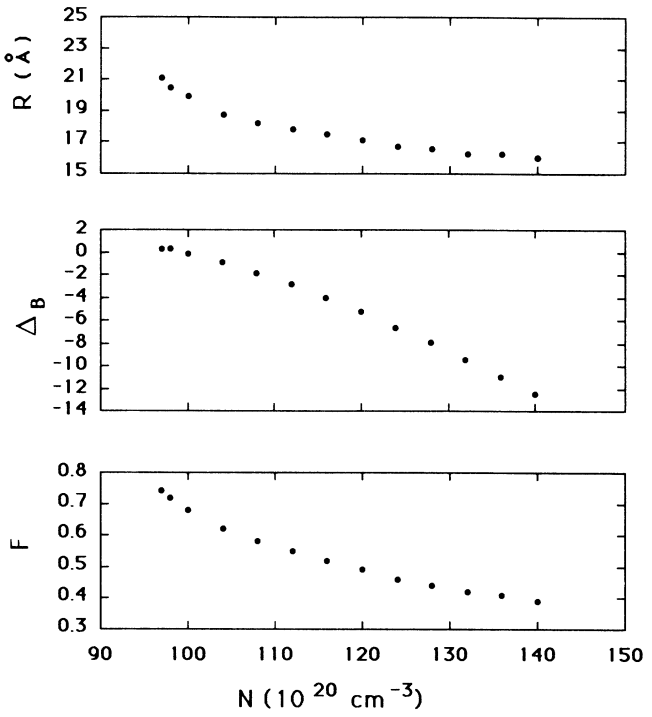

FIG. 14. Bubble radius ($\mathcal{R}$ in Å), Δ_B, and filling factor F plotted vs density at $T=46.5$ K.

radius or of the filling factor. We see from Fig. 13 that a weakly stable bubble can be formed for $N^* \geq 95\times 10^{20}$ cm^{-3}, in fairly good agreement with the experimental results. To give an idea of the various contributions to the total energy $\mathcal{E}_M$, we show them in Table I for $T=46.5$ K, $N=120\times 10^{20}$ cm^{-3}, and $V_0=164.3$ meV.

It has to be said that the results of the model depends on the self-energy $V_0(N)$, for which we do not have at present an unambiguous choice. In spite of its crudeness, however, our model shows that bubble states are possible at the right densities, where we found an enhancement of the decrease of the electron mobility and a peculiar dependence of the mobility on the electric fields. In Fig. 14 we show our results obtained at several densities at $T=46.5$ K with the use of the Wigner-Seitz potential (8).

As said before, we have, at high densities, the coexistence of quasifree and localized states (coexistence region). If $\Delta_B=(\mathcal{E}_B-V_0)/k_BT$, we have as a rough estimate for the number of quasifree and localized electrons, n_F and n_B, $n_F/n_B=\exp(\Delta_B)$, and with $n_F+n_B=n$, $(n_F/n)=\exp(\Delta_B)/[1+\exp(\Delta_B)]$, where n is the total number of electrons. For the average mobility it should be

$$\bar{\mu}=\mu_B(n_B/n)+\mu_F(n_F/n)=\approx\mu_B+(n_F/n)\mu_F\ , \qquad (26)$$

because $\mu_B \ll \mu_F$. We may estimate μ_B as $\mu_B=e/6\pi\eta\mathcal{R}$, where η is the gas viscosity. By neglecting the density dependence of $\mathcal{R}$ and η, we get, with $\mathcal{R}=18$ Å and $\eta=21.0\times 10^{-6}$ Pa s,[26] $\mu_B\approx 2\times 10^{-3}$ cm^{-2}/V s. Extrapolating for μ_F the density dependence of the experimental data for $N<90\times 10^{20}$ cm^{-3}, we get the values shown in Fig. (15).

The disagreement is not surprising, because our system of coexisting quasifree and localized electron states is far from being a simple two-level system. The localization process is, rather, a kind of two-step process. In the first one the electron is trapped in a suitable density fluctuation (incipient bubble).[25] It may then produce a stable bubble in a second step by adjusting the radius and filling density to reach the minimum energy $\mathcal{E}_B$. To calculate the mean mobility $\bar{\mu}$ we need therefore both the mean lifetime of the quasifree electron and the mean stabilization time. No such theory has been produced until now, and the behavior of the electron mobility in the coexistence region is still an open problem.

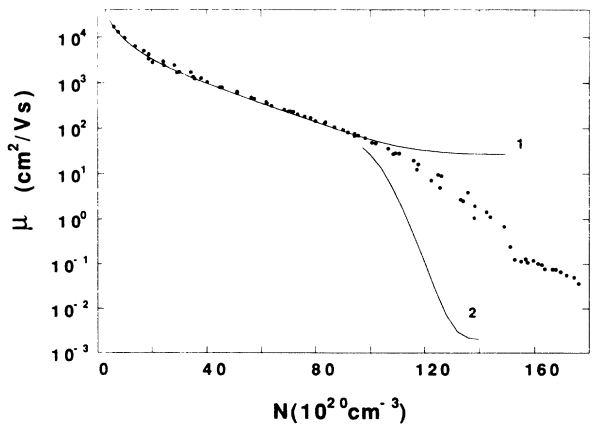

FIG. 15. Experimental mobility results plotted along with the mobility calculated according to Eq. (7), taking into account the energy shift given by Eq. (12) (curve 1). Curve 2 is the average mobility calculated as explained in the text [relation (26)].

ACKNOWLEDGMENTS

The authors acknowledge useful discussions with G. L. Braglia and V. Dallacasa. This work was supported by Consiglio Nazionale delle Richerche and Ministero Università e Ricerca, Rome, Italy.

APPENDIX A

We want to calculate the wave form when the condition $\tau_i \gg \tau_e$ is not satisfied. Let $y = w_e/w_i = \tau_i/\tau_e$, and $i_0 = -en_0/\tau_e$. Let also $y > 1$.

A. $0 \le t \le \tau_e$

The number of electrons present at the time t is $n_e(t) = n_0 \exp(-\nu_A t)$. The number of ions is $n_i(t) = n_0 - n_e(t)$. The total current is $i(t) = en_e(t)/\tau_e - en_i(t)/\tau_i$, which results to be

$$i(t) = \frac{i_0}{y}[1 + (y-1)e^{-Ayt/\tau_i}] , \tag{A1}$$

valid for $0 \le t \le \tau_e$. For $y \gg 1$, the relation (A1) becomes relation (1), Sec. III A.

B. $\tau_e \le t \le \tau_i$

We have only ions, and we need the ionic distribution $n_i(x)$. The number of ions created within $(t', t'+dt')(0 \le t' \le \tau_e)$ is

$$dn_i = \nu_A n_0 e^{-\nu_A t'} dt' = n_i(t')dt' . \tag{A2}$$

They are created at the location $(x', x'+dx')$, with $x' = w_e t'$, $dx' = w_e dt'$. At $t = \tau_e$ these ions are at a new location $(x, x+dx)$, with

$$x = x' + (\tau_e - t')w_i = w_e t' + (\tau_e - t')w_i , \tag{A3A}$$

$$dx = (w_e - w_i)dt' . \tag{A3B}$$

The ionic distribution for $t = \tau_e$ will be $dn_i = n_i(x)dx = n_i(t')dt'$. Inserting t', and dt' from (A3A) and (A3B) one has

$$n_i(x) = n_0 \left[\frac{Ay}{(y-1)d} e^{A/(y-1)} e^{-Axy/d(y-1)} \right] , \tag{A4}$$

which holds for $x_1 \le x \le d$, with $x_1 = w_i \tau_e$. For $x < x_1$, $n_i(x) = 0$. The ionic distribution drifts towards the collector at a velocity w_i. At the time t $(\tau_e \le t \le \tau_i)$, a layer of thickness $d_0 = (t - \tau_e)w_i$ in the front of the distribution has just been collected. The ions in the drift space are therefore

$$n_i(t) = \int_{x_1}^{(d-d_0)} n_i(x)dx ,$$

and they induce a current $i(t) = -en_i(t)/\tau_i$. The calculations give us

$$i(t) = \frac{i_0}{y}(1 - e^{-[Ay/(y-1)][1-t/\tau_i]}) , \tag{A5}$$

which holds for $\tau_e \le t \le \tau_i$.

C. Integrated wave form

Because μ_e is rather low, we can use quite large fields without heating the electronic distribution. In this situation τ_i is small enough to fulfill the condition $RC \gg \tau_i$ ($RC \approx 5$ s). In this case it is easy to obtain the integrated wave form, $v(t) = (1/C)\int_0^t i(t')dt'$. By using the relation (A1), one gets

$$v_1(t) = v_0 \left[\frac{t}{\tau_i} + \frac{y-1}{Ay}(1 - e^{-Ayt/\tau_i}) \right] , \tag{A6}$$

with $v_0 = -en_0/C$. For $t = \tau_e$,

$$v_1(\tau_e) = v_0 \left[\frac{1}{y} + \frac{y-1}{Ay}(1 - e^{-A}) \right] .$$

For $\tau_e \le t \le \tau_i$, $v_2(t) = v_1(\tau_e) + (1/C)\int_{\tau_e}^t i(t')dt'$, where $i(t)$ is now given by (A5). The result is

$$v_2(t) = v_0 \left[\frac{t}{\tau_i} + \frac{y-1}{Ay}(1 - e^{-[Ay/(y-1)][1-t/\tau_i)}) \right] . \tag{A7}$$

For $t = \tau_i$, $v_2(\tau_i) = v_0$. For $t \ge \tau_i$, $v_3 = v_0 \exp[-(t - \tau_i)/RC]$. Two examples of such wave forms are shown in Fig. 16.

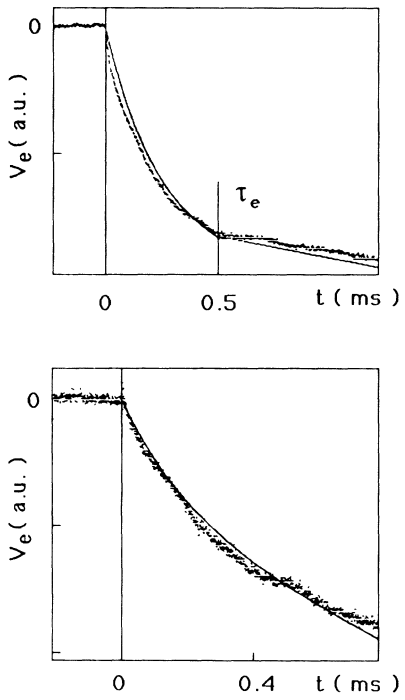

FIG. 16. Two typical wave forms where the electron- to-ion-mobility ratio is small. In the upper signal, obtained with an electric field $E \approx 5230$ V/cm, $\tau_e \approx 660$ μs, $\mu_e/\mu_i \approx 15$. For this wave form the attachment efficiency is $A \approx 2.4$. This value is small enough to detect the kink where the electronic part of the signal ends. In the lower signal, obtained with a field $E \approx 3150$ V/cm, $\tau_e \approx 410$ μs, $\mu_e/\mu_i \approx 4$, the attachment efficiency is $A \approx 25$, so that the discontinuity in the slope at $t = \tau_e$ cannot be detected.

APPENDIX B

We consider a small sphere inside a gas of average density N, enclosed in a volume Ω at a pressure P. Let Ω_i be the initial volume of the small sphere and $N_1=\Omega_i N$ the number of atoms inside it ($\Omega_i \ll \Omega$). Let us force the sphere to expand at $N_1=$const up to a final volume $\Omega_f \ll \Omega$. The mechanical work will be $L=\int_{\Omega_i}^{\Omega_f}[P-p(\Omega')]d\Omega'$, where P and $p(\Omega')$ are the pressure outside and inside the sphere, respectively. The equation of state at $T=$const is usually given as $p=p(n)$, where n is the number density. It is therefore convenient to use $n'=N\Omega_i/\Omega'$ as a new integration variable. if $n_f=N\Omega_i/\Omega_f$ is the final density inside the dilated sphere, we may define a filling factor F as $n_f=FN=(\Omega_i/\Omega_f)N$, and the work can be written as

$$L=N\Omega_i\int_N^{FN}\left[\frac{p(n')}{n'^2}-\frac{P}{n'^2}\right]dn'$$

or

$$L=P\Omega_f\left[(1-F)-\frac{FN}{P}\int_{FN}^{N}\frac{p(n)}{n^2}dn\right]. \tag{B1}$$

The relation (B1) is finally the work needed to create a small spherical bubble of volume Ω_f and density $N'=FN$ inside a gas of density N at the pressure P. In the ideal-gas approximation, $p(n)=nk_BT$, $P=Nk_BT$, and (B1) becomes

$$L=P\Omega_f(1-F+F\ln F). \tag{B2}$$

The ratio $L/P\Omega_f$ is plotted in Fig. 17 as a function of F. One can see that the work done for a partially empty bubble can be considerably smaller than $P\Omega_f$. For $F=0.5$, as an example, the work is only 15% of $P\Omega_f$. The situation is even better for a real gas, as one can see from the results obtained from relation (B1) for neon ($T=46.5$ K, $N=122\times10^{20}$ cm^{-3}, $P\approx3.30$ MPa).

As a check of the correctness of our calculations, we first note that relation (B1) obviously gives $L=P\Omega_f$ for $F=0$. In the second place, we stress the fact that it gives

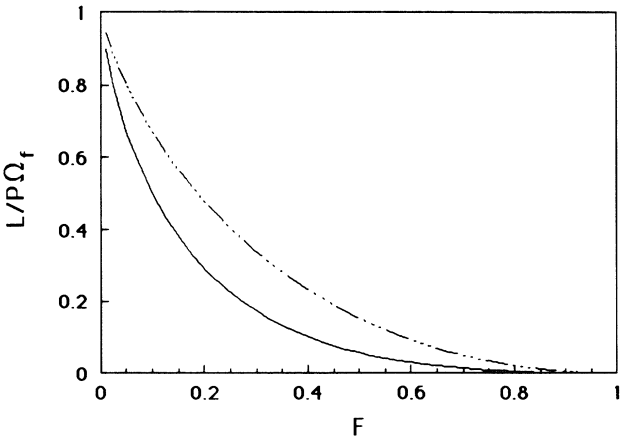

FIG. 17. Ratio of the work spent to create a partially filled spherical cavity of volume Ω_f against the external pressure P as a function of the filling factor F to that done for an empty cavity. Dashed-dotted line, ideal-gas case; solid line, neon gas at $N\approx122\times10^{20}$ cm^{-3} at $T=46.5$ K and at $P\approx3.30$ MPa.

the usual result of the density fluctuations for $F\approx1$ and $(|n-N|/N)\ll1$. In this case, in fact, $p(n)\approx P+\gamma(n-N)$, with $\gamma=(\partial P/\partial n)_{n=N}=(1/n\chi_T)$, where χ_T is the isothermal compressibility. In this approximation it is easy to obtain from (B1) that $L\approx\Omega_f\gamma N[1-F-F\ln(1/F)]$. Expanding $\ln(1/F)$ up to second order, one gets

$$L\approx\Omega_f\gamma N[1-F-F(1/F-1)+0.5F(1/F-1)^2]$$
$$=0.5\Omega_f\gamma N\frac{(1-F)^2}{F}. \tag{B3}$$

Inserting $F=n/N$ and $\gamma=1/N\chi_T$, $L\approx(\Omega_f/2\chi_T)(N-n)^2/nN$, we obtain the usual result for the probability of a thermal density fluctuation[27] $n-N$ inside a volume Ω_f as $\mathcal{P}\propto\exp[-\Omega_f(n-N)^2/2nN\chi_Tk_BT]$.

[1]A. F. Borghesani, L. Bruschi, M. Santini, and G. Torzo, Phys. Rev. A **37**, 4828 (1988).

[2]G. L. Braglia and V. Dallacasa, Phys. Rev. A **26**, 902 (1982).

[3]T. F. O'Malley, J. Phys. B **13**, 1491 (1980); **22**, 3701 (1989).

[4]T. F. O'Malley and R. W. Crompton, J. Phys. B **13**, 3451 (1980).

[5]For helium: J. L. Levine and T. M. Sanders, Phys. Rev. **154**, 138 (1967); H. R. Harrison and B. E. Springett, Phys. Lett. **35A**, 73 (1971). For H_2: H. R. Harrison and B. E. Springett, Chem. Phys. Lett. **10**, 418 (1971).

[6]T. Miyakawa and D. L. Dexter, Phys. Rev. **184**, 166 (1969).

[7]L. Bruschi, G. Mazzi, and M. Santini, Phys. Rev. Lett. **28**, 1504 (1972).

[8]R. J. Loveland, P. G. LeComber, and G. W. Spear, Phys. Rev. B **6**, 3121 (1972).

[9]T. J. Gallagher, *Simple Dielectric Liquids* (Clarendon, Oxford, 1975), p. 22.

[10]CTI Cryogenics, model 21.

[11]A. F. Borghesani, L. Bruschi, M. Santini, and G. Torzo, Rev. Sci. Instrum. **57**, 2234 (1986).

[12]Oxisorb is a trade name of Meissner Greisheim, Düsseldorf, West Germany.

[13]G. Torzo, Rev. Sci. Instrum. **64**, 1162 (1990).

[14]A. F.. Borghesani and M. Santini, Meas. Sci. Technol. **1**, 939 (1990).

[15]OPA 128 Operational amplifier, Burr Brown, Tucson, Arizona.

[16]A. F. Borghesani, L. Bruschi, M. Santini, and G. Torzo, Z. Naturforsch. Teil A **41**, 912 (1986).

[17]R. D. McCarty and R. B. Stewart, National Bureau of

Standards Note No. 8726 (1965) (unpublished).
[18]J. Lekner, Philos. Mag. **18**, 1281 (1968).
[19]For a review see G. L. Braglia and V. Dallacasa, in *Electron and Ion Swarms*, edited by L. G. Christophourou (Pergamon, New York, 1981).
[20]W. Legler, Phys. Lett. **31A**, 129 (1970).
[21]L. L. Foldy, Phys. Rev. **67**, 107 (1945).
[22]E. Merzbacher, *Quantum Mechanics* (Wiley, New York, 1961).
[23]E. Fermi, Il Nuovo Cimento **11**, 157 (1934).
[24]B. E. Springett, J. Jortner, and M. H. Cohen, J. Chem. Phys. **48**, 2720 (1968).
[25]J. P. Hernandez, Phys. Rev. A **7**, 1755 (1973); Phys. Rev. B **11**, 1289 (1975).
[26]V. A. Rabinovich, A. A. Vasserman, V. I. Nedostup, and L. S. Veksler, *Thermophysical Properties of Neon, Argon, and Xenon* (Hemisphere, New York, 1988), p. 358.
[27]R. K. Pathria, *Statistical Mechanics* (Pergamon, New York, 1972), p. 445.

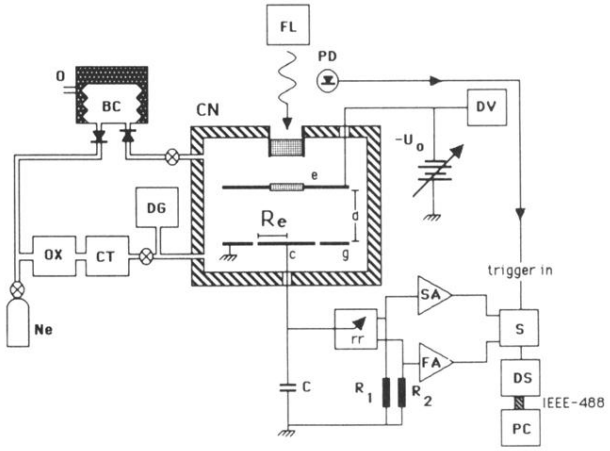

FIG. 1. Schematics of the experimental setup for electron- and ion-mobility measurements in neon gas: FL, xenon flash lamp; PD, photodiode; CN, copper cell; *e*, emitter; *c*, collector; *g*, guard ring; *d*, drift distance; $\mathcal{R}_e$, collector radius; DV, digital voltmeter; *C*, total integration capacitance; $R_1 = 10^{11}\ \Omega$, $R_2 = 10^9\ \Omega$, rr, reed relay; SA, slow amplifier; FA, fast amplifier; SA, selector switch; DS, digital scope; PC, personal computer; CT, liquid-nitrogen-cooled activated charcoal trap; OX, oxisorb trap, Ne, neon flask; *DG*, pressure gauge; IEEE-488, IEEE-488 interface bus.